Cu^{2+} Site in Photosynthetic Bacterial Reaction Centers from *Rhodobacter sphaeroides*, *Rhodobacter capsulatus*, and *Rhodopseudomonas viridis*†

Lisa M. Utschig,* Oleg Poluektov, Sandra L. Schlesselman, Marion C. Thurnauer, and David M. Tiede

Chemistry Division, Argonne National Laboratory, Argonne, Illinois 60439

Received December 22, 2000

ABSTRACT: The interaction of metal ions with isolated photosynthetic reaction centers (RCs) from the purple bacteria *Rhodobacter sphaeroides*, *Rhodobacter capsulatus*, and *Rhodopseudomonas viridis* has been investigated with transient optical and magnetic resonance techniques. In RCs from all species, the electrochromic response of the bacteriopheophytin cofactors associated with $Q_A^-Q_B \rightarrow Q_AQ_B^-$ electron transfer is slowed in the presence of Cu^{2+}. This slowing is similar to the metal ion effect observed for RCs from *Rb. sphaeroides* where Zn^{2+} was bound to a specific site on the surface of the RC [Utschig et al. (1998) *Biochemistry 37*, 8278]. The coordination environments of the Cu^{2+} sites were probed with electron paramagnetic resonance (EPR) spectroscopy, providing the first direct spectroscopic evidence for the existence of a second metal site in RCs from *Rb. capsulatus* and *Rps. viridis*. In the dark, RCs with Cu^{2+} bound to the surface exhibit axially symmetric EPR spectra. Electron spin echo envelope modulation (ESEEM) spectral results indicate multiple weakly hyperfine coupled ^{14}N nuclei in close proximity to Cu^{2+}. These ESEEM spectra resemble those observed for Cu^{2+} RCs from *Rb. sphaeroides* [Utschig et al. (2000) *Biochemistry 39*, 2961] and indicate that two or more histidines ligate the Cu^{2+} at the surface site in each RC. Thus, RCs from *Rb. sphaeroides*, *Rb. capsulatus*, and *Rps. viridis* each have a structurally analogous Cu^{2+} binding site that is involved in modulating the $Q_A^-Q_B \rightarrow Q_AQ_B^-$ electron-transfer process. Inspection of the *Rps. viridis* crystal structure reveals four potential histidine ligands from three different subunits (M16, H178, H72, and L211) located beneath the Q_B binding pocket. The location of these histidines is surprisingly similar to the grouping of four histidine residues (H68, H126, H128, and L211) observed in the *Rb. sphaeroides* RC crystal structure. Further elucidation of these Cu^{2+} sites will provide a means to investigate localized proton entry into the RCs of *Rb. capsulatus* and *Rps. viridis* as well as locate a site of protein motions coupled with electron transfer.

Electron-transfer reactions that occur within proteins are often intimately coupled with other reactions such as conformational changes or proton transfer. Fundamental to understanding biological electron transfer is discerning the involvement of heterogeneous polypeptide environments surrounding the redox cofactor sites in these reaction mechanisms. A useful system to study is that found in photosynthetic bacteria, wherein an integral membrane reaction center (RC)[1] protein couples light-induced sequential electron transfer with proton-transfer reactions (*1, 2*). Proton uptake occurs following the photoexcitation of a special pair of bacteriochlorophylls (P), which decay through a one-electron-transfer reaction via a monomeric bacteriochlorophyll and bacteriopheophytin to the primary (Q_A) and secondary (Q_B) quinone acceptors. After a two-electron, two-proton reduction, Q_BH_2 is released from the RC, transporting electrons and protons to other redox components in the bacteria. In RCs from *Rhodobacter sphaeroides*, the electron transfer between Q_A and Q_B ($Q_A^-Q_B \rightarrow Q_AQ_B^-$) is temperature-activated (*3*−*5*), believed to be rate-limited by protein motion (*6*−*8*), and modulated by metal ions (*9, 10*). $Q_A^-Q_B \rightarrow Q_AQ_B^-$ electron-transfer and Q_B proton-uptake reactions in RCs from different species of purple bacteria have not been as well characterized. We have extended our previous work (*9, 11*) to investigate the metal binding properties of RCs from *Rhodobacter capsulatus* and *Rhodopseudomonas viridis*,[2] specifically searching for a surface metal site involved in electron transfer.

In *Rb. sphaeroides* RCs, metal ion binding to a local protein environment, a Zn^{2+} site on the surface of the RC, has been shown to modulate both electron transfer to Q_B (*9*) and proton uptake by Q_B (*10*). RCs from *Rb. sphaeroides* bind Zn^{2+} stoichiometrically and in a site distinct from the non-heme high-spin Fe^{2+} site, which is buried in the protein interior between Q_A and Q_B. When Zn^{2+} is bound to this site, $Q_A^-Q_B \rightarrow Q_AQ_B^-$ electron transfer is slowed and the room-temperature kinetics become distributed across the microsecond to millisecond time domain (*9*). We proposed

† This work was supported by the U.S. Department of Energy, Office of Basic Energy Sciences, Division of Chemical Sciences, under Contract W-31-109-Eng-38.

* Corresponding author: Chemistry Division D-200, Argonne National Laboratory, 9700 S. Cass Ave., Argonne, IL 60439. Telephone (630) 252-3544; fax (630) 252-9289; e-mail utschig@anl.gov.

[1] Abbreviations: RC, reaction center; P, primary electron donor; Q_A and Q_B, primary and secondary quinone acceptors; cw EPR, continuous wave electron paramagnetic resonance; ESEEM, electron spin echo envelope modulation; EDTA, ethylenediaminetetraacetic acid; LDAO, lauryldimethylamine *N*-oxide; ICP-AES, inductively coupled plasma−atomic emission spectroscopy; ubiquinone$_n$ (UQ_n).

[2] *Rhodopseudomonas viridis* is sometimes referred to as *Blastochloris (Blc.) viridis*.

10.1021/bi0029191 CCC: $20.00
Published on Web 04/26/2001

that Zn^{2+} binding alters the dynamics of conformational changes in the RC, thereby influencing electron transfer (*9*). This work has been extended to show that Zn^{2+} and other metals (including Cd^{2+}, Ni^{2+}, and Co^{2+}) slow electron transfer and also influences the proton uptake of Q_B. A reduction in protonation rate of Q_B indicated one dominant site of proton entry into the RC that is blocked by Zn^{2+} or Cd^{2+} binding (*10*).

A Zn^{2+} site was not observed in the original RC crystal structures of *Rb. sphaeroides* (*12*−*14*). Native surface-bound Zn^{2+} potentially would be eliminated in RC purification and crystallization procedures (*9*). A recent structure obtained with crystals soaked in $ZnSO_4$ has shown the position of the Zn^{2+} to be located near the surface of the protein on the H subunit at a distance of 18 Å away from Q_B (*15*). The Zn^{2+} is coordinated to a cluster of residues, His H126, His H128, and Asp H124, near a water channel proposed as a pathway for proton uptake through the protein matrix (*16*). The position of the metal ion localized the proton entry point near these ligating residues (*15*), and site-directed mutagenesis combined with metal-binding studies has helped elucidate a single favorable interior pathway for proton travel through the *Rb. sphaeroides* RC (*17*).

Experimental proof for the existence of an analogous surface metal ion site has not been reported for RCs from *Rb. capsulatus* or *Rps. viridis*. A similar metal ion site was not observed in the *Rps. viridis* RC structure (*18, 19*). The three-dimensional crystal structure of RC from *Rps. viridis* has been refined to a resolution of 2.3 Å (*20, 21*) and is composed of four polypeptides, namely, L, M, H, and C (a tightly bound tetraheme cytochrome *c*), and 14 cofactors (four heme molecules, four bacteriochlorophyll *b*, two bacteriopheophytin *b*, one carotenoid, one non-heme iron, and two quinones) embedded in the intracytoplasmic membrane. The structure of the RC from *Rb. capsulatus* has not been determined, although site-directed mutagenesis studies coupled with biophysical characterization have been documented (for reviews, see refs *22* and *23*). RCs from *Rb. capsulatus* and *Rb. sphaeroides* share sequence identities of 78%, 76%, and 64% for L, M, and H subunits, respectively, indicating structural homology (*24*). A structural model for L and M subunits and associated cofactors of *Rb. capsulatus* RCs has been calculated (*25*).

Little is known about the proton pathways in RCs from *Rb. capsulatus and Rps. viridis.* Investigation of metal ion interactions at the surface metal site has been instrumental in elucidating the proton pathway into the Q_B site in *Rb. sphaeroides* RCs (*10, 15, 17*), and similar studies may help identify the proton uptake mechanism in these other RCs. RCs need to form hydrogen-bonded networks of ionizable amino acid side chains of L, M, and H protein subunits and bound water molecules for the transfer of protons to doubly reduced Q_B (*26*). Several key residues of the proton pathway determined for RCs from *Rb. sphaeroides* are not conserved in RCs from *Rps. viridis* (*27*). Thus, the functional pathways must be different in these two types of RCs. Some of the bound internal water molecules observed in a refined structure of RCs from *Rps. viridis* could be relevant to the pathways and kinetics of proton transfer to the Q_B site (*28*). Site-directed mutagenesis in RCs of *Rb. capsulatus* and *Rb. sphaeroides* suggests that similar residues may be involved in the electron-transfer-coupled proton-uptake reactions, although more biophysical data is necessary to pinpoint the pathway in *Rb. capsulatus* (*29*). Fourier transform infrared (FTIR) experiments demonstrated that the Q_B environment of RCs from *Rb. capsulatus* varies slightly from that observed in *Rb. sphaeroides* RCs, suggesting subtle differences in the peptide and internal water structures (*30*).

In addition to proton-transfer events, metal ion binding studies may provide insight into conformational changes important for electron transfer. In RCs from *Rb. sphaeroides*, the first electron-transfer step involves a slow rate-limiting gating step (*16*) that involves the movement of Q_B before electron transfer (*8*). Other evidence suggests that k_{AB} is limited by a conformational change (*5, 31, 32*). Upon stoichiometric Zn^{2+} or Cd^{2+} binding, the rate of electron transfer is slowed, implying a change in protein dynamics due to a conformational change, or a slowing down of the conformational gating step (*9, 10*). Comparison of the RC structure with or without Cd^{2+} bound indicated mobility difference in a specific residue, and this residue has been proposed to be involved in the reduced rate of electron transfer (*15*).

One potential method for detecting protein conformational changes is to spectroscopically probe the dynamic solution metal site structure. Herein, we report procedures for binding Cu^{2+} to isolated Fe-containing RCs from *Rb. capsulatus* and *Rps. viridis*. We have used transient optical measurements to determine the influence of Cu^{2+} on the electron-transfer properties along with magnetic resonance techniques to interrogate the electronic structure of the RC Cu^{2+} sites and surrounding protein in these RCs. Recently we reported procedures for stoichiometrically binding Cu^{2+} to RCs from *Rb. sphaeroides*, and we showed with cw and pulsed EPR that the Cu^{2+} binds to two or more histidine ligands at a surface site of the RC (*11*). We have extended this work to include the Cu^{2+}-induced electrochromic response of the bacteriopheophytin cofactors associated with $Q_A^-Q_B \rightarrow Q_AQ_B^-$ electron-transfer and/or charge-compensating (proton-uptake) events for RCs from *Rb. sphaeroides*, *Rb. capsulatus*, and *Rps. viridis*.

Concomitant with these kinetic experiments, spectroscopic determination of the nature and geometry of the ligands at the Cu^{2+} site will be important for understanding the mechanism of metal ion-induced modulation of electron and proton transfer. Thus, electron spin echo envelope modulation (ESEEM) spectroscopy was used to characterize the magnetic interactions between Cu^{2+} and weakly coupled magnetic nuclei in these RCs. ESEEM spectroscopy is a particularly useful method for probing Cu^{2+}−imidazole interactions in Cu-containing metalloproteins (*33*−*35*). With this technique one observes periodicities (modulations) in the ESEEM envelope that arise from the interaction of the unpaired electron spin of Cu^{2+} with the nuclear spins of the so-called remote nitrogens of the Cu^{2+} ligating histidines (*36*). In this paper we present our initial characterization of Cu−RCs from *Rps. viridis* and *Rb. capsulatus* by ESEEM and cw EPR spectroscopy. These spectra provide the first direct spectroscopic evidence of a second metal site on these RCs. Further elucidation of these Cu^{2+} sites may provide a means to investigate localized proton entry into the RCs of *Rb. capsulatus* and *Rps. viridis* as well as determine a generalized functional role of a local metal ion site in modulating electron transport.

EXPERIMENTAL PROCEDURES

Preparation of Rps. viridis RCs. Purified RCs from *Rps. viridis* were prepared as described previously (*37*). Chromatophores (absorbance of 50 cm^{-1} at 1015 nm) were suspended in 10 mM Tris-HCl, pH 7.7, and 10 μM EDTA and incubated for 7 min with 5% LDAO at room temperature. The LDAO extract was then loaded onto a sucrose gradient (0.1−1 M sucrose, 0.1% LDAO, 1 mM EDTA, and 10 mM Tris-HCl, pH 7.8) and spun at 160000*g* for 18 h. The RC band was collected and loaded onto a DEAE-Sephacel column equilibrated with 10 mM Tris-HCl, pH 7.9, 1 mM EDTA, and 0.1% LDAO. The RCs were eluted with a 0−0.10 M NaCl gradient. RCs with A_{280}/A_{830} ratios of 2.1−2.4 were collected and concentrated with Centriprep-50 (Amicon) devices.

For Cu^{2+} binding experiments, RCs were dialyzed into buffer containing 10 mM HEPES, pH 7.9, 20 mM NaCl, and 0.045% LDAO. The RC protein ($OD_{830} \sim 14$ cm^{-1}) was incubated with ~10 mol equiv of $CuSO_4$ at ice temperature for 3 h. Free Cu^{2+} was separated from bound metal ion by gel-filtration chromatography through a Sephadex G-25 (Pharmacia) column equilibrated with 10 mM HEPES at pH 7.9, 20 mM NaCl, and 0.045% LDAO.

Preparation of Rb. capsulatus RCs. RCs were purified from *Rb. capsulatus* on the basis of published procedures (*38*). Chromatophores (absorbance of 9.5 cm^{-1} at 876 nm) were suspended in 10 mM Tris-HCl, pH 7.8, and 100 mM NaCl and incubated for 9 min with 0.7% LDAO at 33 °C. RCs were precipitated from the extract following addition of 32% $(NH_4)_2SO_4$. The pellet was resuspended in 10 mM Tris-HCl, pH 8.0, 10 μM EDTA, 50 mM NaCl, and 0.15% LDAO and loaded onto a sucrose gradient (12−36% sucrose, 0.04% LDAO, 10 μM EDTA, and 10 mM Tris-HCl, pH 7.8) and spun at 160000*g* for 16 h. The RC band was collected and dialyzed vs 10 mM Tris-HCl, pH 7.8, 10 μM EDTA, and 0.04% LDAO at 4 °C overnight. RCs were loaded onto a DEAE-Sephacel column equilibrated with 20 mM Tris-HCl, pH 8.0, 20 μM EDTA, and 0.045% LDAO. The RCs were eluted with a 30 mM−0.20 M NaCl gradient. RCs with A_{280}/A_{800} ratios of 1.7−2.0 were collected and concentrated with Centriprep-50 (Amicon) devices. Specific variations were made to the protocol in order to achieve less pure, yet hopefully more native, intact RCs (*5*). Reconstitution of RCs (A_{280}/A_{800} ratios of 1.2) with UQ_{10} was difficult and inconsistent transient optical measurements were observed, although stoichiometric Cu−RCs with purities of 1.2 vs 1.7 resulted in identical cw EPR spectra. Azide was absent from all preparation buffers. RCs purified in the presence of azide, even after extensive dialysis with azide-free buffer, degraded in the presence of $CuSO_4$, suggesting residual azide is integrated into the protein.

For Cu^{2+} binding experiments, RCs were dialyzed into buffer containing 10 mM HEPES, pH 7.86, 20 mM NaCl, and 0.045% LDAO. RCs were incubated with 5 equiv of Cu^{2+} for 1 h on ice and then passed through a Sephadex G25 column to remove unbound Cu^{2+} from Cu−RC complexes. Centriprep-50 devices were used to concentrate the RCs. EPR samples were dark-adapted, frozen, and stored in liquid N_2.

Preparation of Rb. sphaeroides RCs. RCs were purified from cells of *Rb. sphaeroides* R26 (*39*). Stoichiometric Cu−RC complexes were prepared by gel-filtration procedures as previously detailed (*11*).

Metal Analysis. Inductively coupled plasma−atomic emission spectroscopy (ICP-AES) on a Thermo Jarell Ash Atomscan Advantage spectrometer was used to determine the amount of Cu bound to the RC. The ICP-AES instrument is equipped with an axial plasma configuration. The analytical standard deviation for these measurements was ~0.01.

Transient Optical Spectroscopy. The rate of $Q_A^-Q_B \rightarrow Q_AQ_B^-$ first electron transfer was measured at 750 nm (*Rb. capsulatus*), 755 nm (*Rb. sphaeroides*), or 810 and 850 nm (*Rps. viridis*) by monitoring the absorbance changes in the bacteriopheophytin electrochromic band shift, which is sensitive to the reduction state of Q_A and Q_B (*5*, *41*, *43*). Optical absorption changes were identified by recording kinetic traces as a function of time after a 5 ns, 20 mJ laser excitation pulse at 594 nm (OPOTEK Inc). The probe light, placed perpendicular to the excitation light, was from a 50 W halogen−quartz tungsten lamp (Wilmad) passed through a monochromator and was controlled by a shutter placed before the RC sample that was only opened during measurement. The avalanche photodiode (RCA) was protected from the actinic light by a second monochromator tuned to match the first, and the output signal was sent to a Tektronix TDS 350 digital storage oscillosope. Eight to 32 transients were averaged to improve signal-to-noise. For RCs from *Rb. sphaeroides* and *Rb. capsulatus*, charge recombination rates were measured by monitoring the recovery of the donor band at 860 nm after bleaching with a single 594 nm laser flash. In addition to single wavelength measurements, transient spectra as a function of time between a 5 ns laser excitation pulse at 614 nm and a weak 0.65 μs xenon probe pulse were obtained for *Rps. viridis* RCs, by use of a 1024 element, single diode array, multiwavelength detector. The experimental setup has been described previously (*5*). All spectra were obtained at 21 °C.

For *Rb. sphaeroides* RCs, Q_B was reconstituted by adding quinone (200 μM; ~10 equiv/RC) from a stock solution containing 2 mM $ubiquinone_{10}$ (Sigma) and 1% LDAO that had been heated to 65 °C for approximately 5 min. Similarly, $ubiquinone_6$ (Sigma) was used to reconstitute *Rb. capsulatus* RCs. Greater than 85% of the *Rb. capsulatus* RCs ($A_{280}/A_{800} \sim 1.7$) was reconstituted by simply adding 10 equiv of quinone/RC at room temperature. In contrast, *Rb. capsulatus* RCs with higher purity ($A_{280}/A_{800} \sim 1.2$) were difficult to reconstitute. Incubating these RCs with 50 equiv of UQ_6 for 20 min at 30 °C in the presence of 100 mM NaCl resulted in only 60−70% reconstitution, and significantly slower $Q_A^-Q_B \rightarrow Q_AQ_B^-$ electron-transfer rates were observed. Optical experiments for *Rps. viridis* RCs were obtained in the presence of 10 equiv of UQ_{10}/RC and 200 μM quinhydrone (Kodak). Absorbance changes at 960 nm were measured and indicated that the bound cytochrome effectively rereduced P^+ within our instrument response time.

EPR Spectroscopy. Continuous-wave EPR spectra were obtained to observe the first-derivative Cu^{2+} signals. The X-band data were collected on a Bruker ESP300E EPR spectrometer with a Bruker X-band ER046XK-T bridge. Spectra were measured at 10 K.

Pulsed EPR experiments were performed on a home-built homodyne pulsed X-band EPR spectrometer, previously described (*11*). A Bruker dielectric cavity (ER4118X-MD5)

was employed. The ESEEM experiments were performed at liquid helium temperature with a three-pulse ($\pi/2-\tau-\pi/2-T-\pi/2$) stimulated echo pulse sequence. Spectra were collected at a τ value of 180 ns for each data set containing 512 points, at a magnetic field of 3340 G. The repetition rate of the applied pulse sequence was 100 Hz, with a microwave frequency of 9.57 GHz, and a pulse width of 20 ns.

RESULTS

Binding of Cu^{2+} to RCs. Previously, we have shown that stoichiometric Cu−RC complexes (Cu/RC mole ratio of 1) from *Rb. sphaeroides* can be readily obtained by incubating purified RCs with several equivalents of $CuSO_4$ followed by gel-filtration chromatography or extensive dialysis to remove unbound metal ion (*11*). We have extended our metal binding studies to include RCs from *Rb. capsulatus* and *Rps. viridis*. Isolated, purified RCs from each species contained less than 0.1 mol equiv of Cu^{2+}/RC, as determined by metal analysis. Addition of excess Cu^{2+} followed by gel-filtration chromatography provided the most consistent methods for forming near-stoichiometric Cu−RC complexes. By this method, Cu/RC mole ratios of ∼1.3 and ∼1.0 were determined for RCs from *Rb. capsulatus* and *Rps. viridis*, respectively. Repeated attempts to bind Zn^{2+} to *Rps. viridis* RCs were unsuccessful.

The Cu^{2+} does not displace the non-heme Fe^{2+}, which is located between Q_A and Q_B. These Cu−RC samples were simply prepared by the addition of excess metal ion to native, Fe-containing RCs. In contrast, specific, stringent conditions (i.e., chaotropic treatment) are necessary to remove and replace the non-heme Fe^{2+}, which is buried in the interior of the RC protein (*39, 40*). Metal analysis shows that RCs retain Fe^{2+} after the Cu^{2+} is bound by gel-filtration procedures, with measured average metal-to-protein ratios of 1 Fe/RC and 5 Fe/RC for *Rb. capsulatus* and *Rps. viridis*, respectively. The procedures for binding Cu^{2+} to *Rps. viridis* and *Rb. capsulatus* are similar to those for binding Zn^{2+} and Cu^{2+} to *Rb. sphaeroides* RCs, where it has been shown that Zn^{2+} and Cu^{2+} are "surface accessible" (*9, 11, 15*). We assert that the Cu^{2+} sites on RCs from *Rb. capsulatus* and *Rps. viridis* are similarly "surface accessible".

Transient Optical Measurements: (A) Rb. sphaeroides. Transient optical measurements show that the $Q_A^-Q_B \rightarrow Q_AQ_B^-$ electron-transfer rate is reduced in the presence of excess Cu^{2+} for RCs from *Rb. sphaeroides*. The kinetics of absorbance changes in the electrochromic response associated with $Q_A^-Q_B \rightarrow Q_AQ_B^-$ electron transfer in the *Rb. sphaeroides* RCs have been well characterized (*3, 5, 41*). Optical measurements at 755 nm in isolated RCs have been primarily assigned to electron transfer, whereas electrochromic responses at other wavelengths indicate a combination of electron-transfer and charge-compensating events, such as proton transfer (*41*). Figure 1 shows the time course for absorbance changes associated with the $Q_A^-Q_B \rightarrow Q_AQ_B^-$ electron transfer for RCs in the presence and absence of Cu^{2+}. Like Zn^{2+} and Cd^{2+}, in the presence of Cu^{2+} $Q_A^-Q_B \rightarrow Q_AQ_B^-$ electron transfer is slowed. In native RCs with no extraneous metal ion, $Q_A^-Q_B \rightarrow Q_AQ_B^-$ electron-transfer rate is heterogeneous at room temperature, consisting of at least two distinct components (*5*). For RCs in the absence of Cu^{2+},

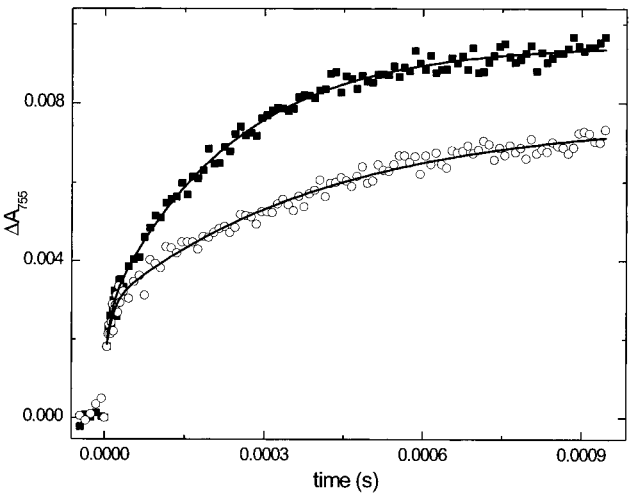

FIGURE 1: Time course for absorbance changes associated with the $Q_A^-Q_B \rightarrow Q_AQ_B^-$ electron-transfer process in RCs from *Rb. sphaeroides*. Optical absorption changes at 755 nm associated with quinone anions in transient P^+Q^- states were obtained for RCs in the absence (■) and presence (○) of 10 mol equiv of $CuSO_4$ at 21 °C. Biexponential fits of the data are shown (solid lines).

we measured a major component (73%) with reaction time of 220 ± 30 μs and a minor component (27%) with reaction time of 10 ± 1 μs. The same preparation of RCs in the presence of excess Cu^{2+} yielded biexponential fits with lifetimes of 425 ± 5 μs (70%) and 20 ± 10 μs (30%). Thus, the slowest component of $Q_A^-Q_B \rightarrow Q_AQ_B^-$ electron transfer of Cu−RCs is markedly longer than the ∼200 μs slowest component observed in native, non-Cu-containing RCs. When Cu^{2+} is stoichiometrically bound by gel filtration (0.9 Cu/RC), similar kinetics were observed: 360 ± 30 μs (66%) and 30 ± 5 μs (34%). No significant difference in the $P^+Q_A^-$ and $P^+Q_B^-$ room-temperature recombination rates for RCs with or without Cu^{2+} bound was observed. $P^+Q_A^- \rightarrow PQ_A$ rates of $(0.13 \pm 0.02\ s)^{-1}$ and $(0.14 \pm 0.07\ s)^{-1}$ were measured for RCs with and without Cu^{2+}, respectively. The $P^+Q_B^- \rightarrow PQ_B$ rates of $(1.08 \pm 0.13\ s)^{-1}$ and $(1.16 \pm 0.03\ s)^{-1}$ were observed for RCs with and without Cu^{2+}. Apparently, Cu^{2+} does not slow electron transfer to the same extent as Zn^{2+}, where the slowest component was on the order of 1 ms (*9*). However, the multiphasic nature of the $Q_A^-Q_B \rightarrow Q_AQ_B^-$ electron-transfer step makes a simple interpretation of these results difficult. Depending on the mechanism of metal-induced modulation of electron transfer, one possibility is that Cu^{2+} is binding in a different coordination geometry than Zn^{2+}, thereby influencing electron transfer to a different extent.

(B) Rb. capsulatus. The influence of Cu^{2+} on the $Q_A^-Q_B \rightarrow Q_AQ_B^-$ electron-transfer rate is strikingly similar for RCs from *Rb. capsulatus* and *Rb. sphaeroides* RCs. The measurements obtained at 750 nm are shown in Figure 2. The absence of an absorbance change increase in the presence of stigmatellin is consistent with attributing the observed kinetics to the $Q_A^-Q_B \rightarrow Q_AQ_B^-$ electron-transfer process. The kinetics of absorbance changes in the electrochromic response associated with $Q_A^-Q_B \rightarrow Q_AQ_B^-$ electron transfer are slowed in the presence of Cu^{2+}. At pH 7.8, in the absence of added metal ion, biexponential room-temperature kinetics were observed, yielding lifetimes of 105 ± 3 μs (79%) and 10 ± 2 μs (21%). The observed longest component is the same order of magnitude as the previously reported

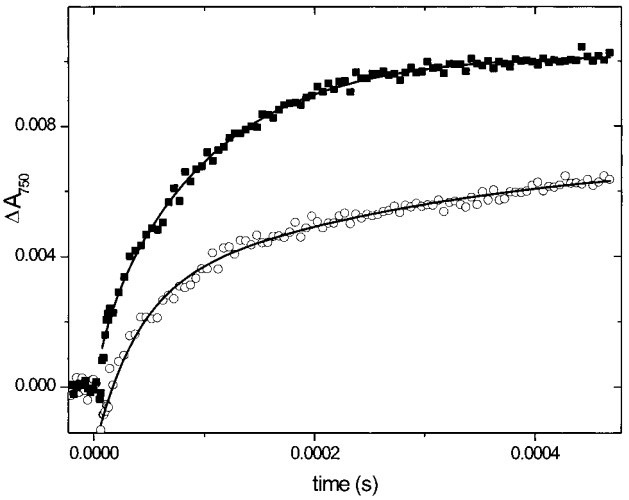

FIGURE 2: Time course for absorbance changes associated with the $Q_A^-Q_B \rightarrow Q_AQ_B^-$ electron-transfer process in RCs from *Rb. capsulatus*. Optical absorption changes at 750 nm associated with quinone anions in transient P^+Q^- states were obtained for RCs in the absence (■) and presence (○) of 17 mol equiv of $CuSO_4$ at 21 °C. Biexponential fits of the data are shown (solid lines).

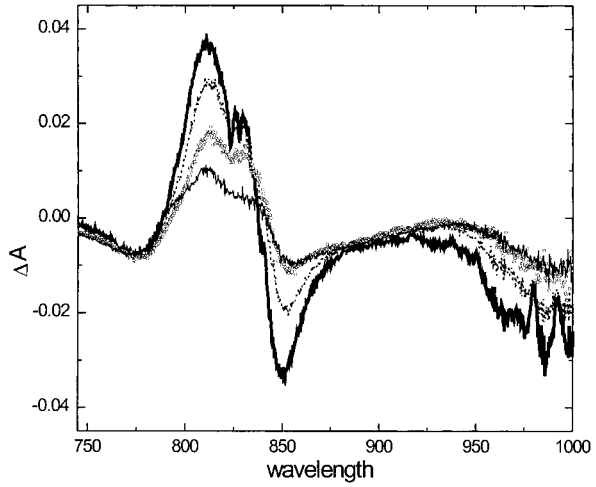

FIGURE 3: Transient PQ^- − PQ difference spectra measured at room temperature in isolated *Rps. viridis* RCs with 0 s (bold line), 1 μs (dotted line), 10 μs (open circles), and 100 μs (thin line) time delays following laser excitation.

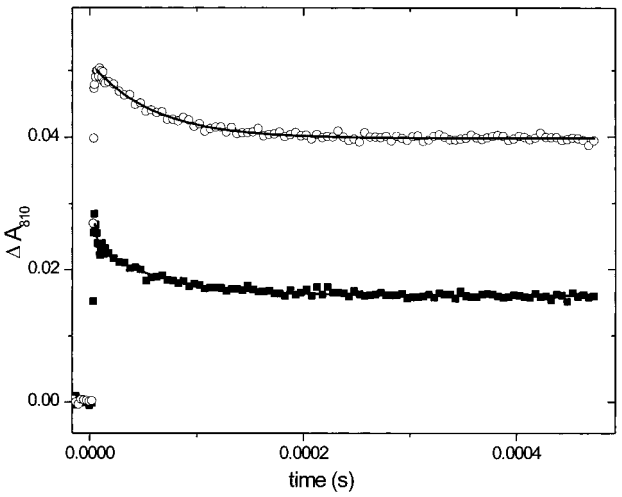

FIGURE 4: Time course for absorbance changes associated with the electrochromic response of the bacteriopheophytin in RCs from *Rps. viridis*. Optical absorption changes at 810 nm associated with quinone anions in transient PQ^- states were obtained for RCs in the absence (■) and presence (○) of 17 mol equiv of $CuSO_4$ at 21 °C. A biexponential fit of the data is shown (solid lines) for RCs in the absence of Cu^{2+}. The kinetics observed in the presence of Cu^{2+} were fit with a single exponential.

65 ± 10 μs lifetime obtained with a single-exponential fit for *Rb. capsulatus* RCs at pH 7.0 (*42*). In the presence of excess Cu^{2+}, both the observed slow and fast components increase, with biexponential fits resulting in lifetimes of 300 ± 90 μs (50%) and 40 ± 4 μs (50%). A slight difference in the $P^+Q_B^-$ room-temperature recombination rates for RCs with or without metal ion present was observed. The $P^+Q_B^-$ room-temperature recombination rates appeared to increase somewhat with rates of $(0.79 \pm 0.06\ s)^{-1}$ and $(1.10 \pm 0.21\ s)^{-1}$ for RCs in the absence or presence of Cu^{2+}. These changes may indicate possible electrostatic or structural changes near Q_B upon Cu^{2+} binding (*10*). $P^+Q_A^-$ recombination rates were similar, with observed rates of $(0.10 \pm 0.02\ s)^{-1}$ and $(0.13 \pm 0.02\ s)^{-1}$ for RCs in the absence or presence of Cu^{2+}, respectively.

(C) Rps. viridis. In *Rps. viridis*, the electron transfer from Q_A to Q_B is not as well-characterized as that in *Rb. sphaeroides*. The induced electrogenic absorption shifts in bacteriopheophytin due to reduced quinones have been studied in detail by Shopes and Wraight (*43*). Figure 3 shows the time-resolved electrochromism associated with the formation of quinone anions in *Rps. viridis* RCs. A change in the amplitude of the electrogenic response, but no distinct time-resolved absorption shift, is observed. Thus, the observed time-resolved electrochromism associated with the formation of quinone anions in the *Rps. viridis* RCs is complicated and cannot be easily ascribed to purely electron transfer. The observed attenuation of the electrochromism could result from either charge compensation, i.e., quenching by proton (or other counterion) movement near Q_A^- or Q_B^-, and/or electron transfer between the quinones.

Nevertheless, Cu^{2+} influences the electrochromic response in isolated RCs from *Rps. viridis* as shown in Figure 4. In native RCs with no extraneous metal ion, the observed response at 810 nm is heterogeneous at room temperature consisting of a major fast component (70%) with reaction time near that of our instrument response time of 5 ± 1 μs and a minor component (30%) with reaction time of 65 ± 5 μs. In the presence of Cu^{2+}, the fast component is lost and the reaction kinetics can be fit with a single exponential with a lifetime of 60 ± 2 μs. A change in the rates was also observed at 850 nm. Without metal present, the reaction happens faster than the instrument response time, <2 μs, but in the presence of Cu^{2+} a slow component emerges with a lifetime of 150 ± 20 μs. In addition, Cu^{2+} induces some changes in the ultrafast RC kinetics. At the time scale of the laser pulse, RCs in the presence of Cu^{2+} have nearly twice the absorbance change compared to RCs with no metal ion present. These dramatic changes in the early events will be investigated with faster time resolution instrumentation. Previously measured kinetics of the decay of the absorption shift at 830 nm yielded a half-time of about 25 μs (*44*, *45*). The transient optical results for the three species are summarized in Table 1.

CW EPR. We have used Cu^{2+} ($3\ d^9$, $S = {}^1/_2$) to probe the electronic structure of the RC surface metal sites and their local protein environments. All of our Cu−RC samples

Table 1: Summary of Exponential Amplitude and Lifetime Parameters Used To Fit Absorbance Changes Due to Electrochromic Response of Bacteriopheophytin to Q_A^- and Q_B^- in Isolated RCs

	no metal	$+Cu^{2+}$
Rb. sphaeroides RCs	220 ± 30 μs (73%)	425 ± 5 μs (70%)
	10 ± 1 μs (27%)	20 ± 10 μs (30%)
Rb. capsulatus RCs	105 ± 3 μs (79%)	300 ± 90 μs (50%)
	10 ± 2 μs (21%)	40 ± 4 μs (50%)
Rps. viridis RCs	65 ± 5 μs (30%)	60 ± 2 μs (100%)
	5 ± 1 μs (70%)	

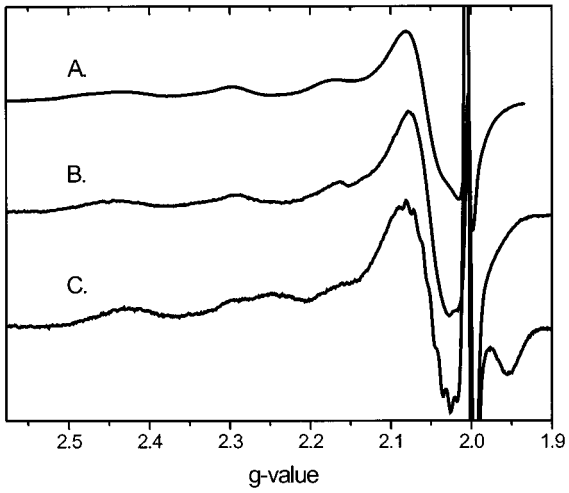

FIGURE 5: X-band EPR spectra of Cu−RCs, recorded in the dark at 10 K. (A) Spectrum of Cu^{2+} RCs (0.9 Cu/0.9 Fe/RC) from *Rb. sphaeroides*, taken from ref *11*. (B) Spectrum of RCs from *Rb. capsulatus* (1.3 Cu/1.2 Fe/RC) by gel-filtration chromatography and concentrated to $OD_{800} = 30$ cm^{-1} ($A_{280}/A_{800} = 1.7$). (C) Spectrum of RCs from *Rps. viridis* (1.0 Cu/5 Fe/RC) by gel-filtration chromatography and concentrated to $OD_{830} = 40$ cm^{-1} ($A_{280}/A_{830} = 2.1$). The data were collected at 9.14 GHz, with 10 G modulation amplitude, 0.2 mW microwave power, and 100 kHz modulation frequency.

contain copper in natural isotopic abundance (^{63}Cu 69.1%, ^{65}Cu 30.1%). Both isotopes have nuclear spins with $I = {}^3/_2$ and magnetic moments differing by 6.6%. Therefore, two magnetic isotopes contribute to each spectrum. Recently, we reported EPR data on RCs where Cu^{2+} was bound to the surface site on native Fe^{2+}-containing *Rb. sphaeroides* RCs and to the native non-heme Fe site in biochemically Fe-removed RCs (*11*). The cw and pulsed EPR results clearly indicated two spectroscopically different Cu^{2+} environments. These results provide a benchmark for comparison of the RCs from different species with Cu^{2+} bound to surface site(s).

The EPR spectra of Cu^{2+}−RC complexes (native Fe-containing) prepared via gel-filtration methods for three different species of RCs are shown in Figure 5. In each spectrum, four peaks arising from the hyperfine coupling of the unpaired spin of Cu^{2+} with the nuclear spin of the Cu (^{65}Cu and ^{63}Cu) are observed at low magnetic field. The *g*-values and hyperfine constants differ for each species (Table 2). For *Rb. capsulatus* RCs, the Cu^{2+} site exhibits an axially symmetric EPR spectrum with $g_{||} = 2.22$, $A_{||} = 179$ G, and $g_\perp = 2.06$. This spectrum is similar to that of *Rb. sphaeroides*, with $g_{||} = 2.24$, $A_{||} = 160$ G, and $g_\perp = 2.06$, which is consistent with tetragonal symmetry for the coordinated ligands (*46*−*48*). In *Rb. capsulatus* and *Rb. sphaeroides*, resolved nitrogen hyperfine coupling in $g_{||}$ and $g_\perp$ was not observed (this coupling is not commonly observed in Cu proteins), a result of overlapping ^{65}Cu and ^{63}Cu resonances or a disordered metal site. The observed spectrum is typical of type 2 or "normal" copper EPR signals (*49*), having *g* and *A* values characteristic of most cupric complexes. A residual dark signal from P^+ is observed at $g = 2.0026$ in each spectrum.

Table 2: Summary of EPR Parameters Observed for Cu^{2+} RCs at cw X-band

	$g_{||}$	$A_{||}$(G)	$g_\perp$
Cu_{sur}-RCs[a]			
Rb. sphaeroides	2.24	160	2.06
Rb. capsulatus	2.22	179	2.06
Rps. viridis	2.23	164	2.06
	2.17	211	2.06
Cu_{FeQ}-RC[b]			
Rb. sphaeroides	2.31	143	2.07

[a] Cu bound to native Fe-containing RCs by gel-filtration chromatography. [b] Cu bound to the Fe site in Fe-removed RCs prepared with chaotropic methods (*11*).

The spectrum of *Rps. viridis* RCs is different, exhibiting signals from two spectroscopically distinct Cu^{2+} environments. Spectral simulations result in one Cu^{2+} with parameters $g_{||} = 2.23$, $A_{||} = 164$ G, and $g_\perp = 2.06$, similar to the values observed for RCs from *Rb. sphaeroides* and *Rb. capsulatus*. Resolved hyperfine coupling to 3−4 coordinated nitrogens is observed for a second Cu^{2+}. The values of $g_{||} = 2.17$, $A_{||} = 211$ G, $A_\perp = 15$ G, and $g_\perp = 2.06$ are strikingly similar to those reported by Buchanan and Dismukes (*50*) for RCs from *Rb. sphaeroides* (strain Y) that had biosynthetically incorporated Cu^{2+} into the Fe site. Metal analysis confirms that Fe is present in the non-heme Fe site in our *Rps. viridis* samples. These parameters suggest a tetragonal coordination environment for the Cu^{2+} (*48*). Identical Cu^{2+} spectra have been observed for three different sample preparations. The light-induced EPR spectrum is essentially unchanged from the dark spectrum shown in Figure 5. Thus, both Cu^{2+} "sites" are in a remote position from Q_A^-. It is feasible that the spectra reflect Cu^{2+} binding at the same location on the RC but in two distinct coordination environments, i.e., different geometry or number of ligands. Interestingly, we observed temperature-dependent conformational flexibility of the first Cu^{2+}-type environment. Elaboration of this dynamic process as well as further characterization of the second type of Cu^{2+} environment will be presented in a future paper (O. Poluektov and L. M. Utschig, unpublished results).

Each spectrum has noticeably different hyperfine coupling and **g** tensors than the spectrum of Cu^{2+} biochemically bound to the Fe site (*11*, *51*, *52*), which has $A_{||} = 143$ G. The **g** tensor is typical for Cu^{2+} in axial symmetry, corresponding to a $d_{x^2-y^2}$ ground-state orbital for the unpaired electron, with $g_{||} = 2.31$ and $g_\perp = 2.07$. By analogy with the X-ray structure of the Fe site (*12*−*14*), Cu^{2+} could be coordinated by four histidine residues (two each from the L and M subunits) and to one glutamic acid acting as a bidentate ligand. From analysis of the superhyperfine interaction with ^{14}N and ^{15}N in ^{65}Cu-enriched samples, Calvo et al. (*52*) concluded that only three histidine ligands are directly coordinated to the Cu^{2+}.

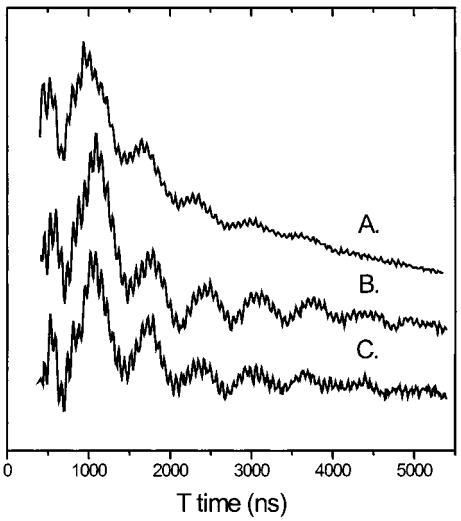

FIGURE 6: Three-pulse ESEEM spectra of Cu−RCs from (A) *Rb. sphaeroides* (*11*), (B) *Rb. capsulatus*, and (C) *Rps. viridis*. The time domain spectra are displayed. Experimental parameters: magnetic field 3340 G, microwave frequency 9.57 GHz, pulse width 20 ns, $\tau = 180$ ns, repetition rate 100 Hz, temperature 4 K.

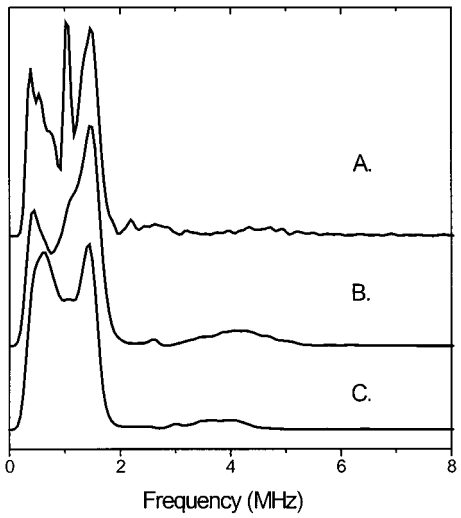

FIGURE 7: Fourier transforms of the three-pulse time domain ESEEM spectra shown in Figure 6.

ESEEM Spectroscopy. Electron spin echo envelope modulation (ESEEM) spectroscopy was used to examine the nature of the ligands at the Cu^{2+} site (*33*−*35*). Three-pulse ESEEM spectra of Cu^{2+}-substituted RCs are presented in Figure 6. The magnetic field for the time-domain ESEEM data shown was set at the maximal three-pulse echo-induced field-swept (ESE) EPR intensity for the observed signal at $g = 2.06$. Figure 7 displays the Fourier transforms of the time-domain ESEEM data. For comparison, we show the ESEEM spectra previously reported for Cu−RCs from *Rb. sphaeroides* (*11*). The observed spectra resemble spectra obtained for Cu^{2+}−imidazole model compounds (*36, 53*−*55*) and for several Cu^{2+}−proteins (*56*−*67*).

In each spectra, intense peaks in the 0.4−1.5 MHz region were observed. At a magnetic field of the maximum ESE-detected EPR spectrum, Cu−RCs from *Rb. capsulatus* reveal two intense peaks at 0.43 and 1.46 MHz, with a shoulder at 1.12 MHz, indicating several overlapping peaks. Likewise, *Rps. viridis* Cu^{2+}−RCs exhibit two major peaks at 0.60 and 1.43 MHz, with a smaller peak at 1.06 MHz. Spectral deconvolution indicates that these peaks represent the sum of at least five smaller peaks. Interestingly, the frequencies of each of the five peaks were identical for spectra obtained for the three RC species. Such spectral features are characteristic of weakly hyperfine-coupled ^{14}N nuclei in close proximity to a paramagnetic species (Cu^{2+}) near the "exact cancellation" limit (*36, 68*). At this limit, in one of the electron spin manifolds, the splitting of the ^{14}N nuclear Zeeman interaction is canceled by that of the hyperfine interaction, typically giving rise to three low-frequency transitions below 2 MHz (*36*). These transition frequencies arise from the ^{14}N nuclear quadrupole interaction (nqi) and are invariant with applied magnetic field. Other features of the ESEEM spectrum include several shallow overlapping bands with peaks at 3.3, 4.0, and 4.4 MHz. Very low intensity, overlapping peaks are observed, centered at ∼4.1 and ∼3.8 MHz for *Rb. capsulatus* and *Rps. viridis*, respectively. These peaks move linearly with the magnetic field and correspond to the $\Delta M_I = 2$ transition, which exhibits a typical frequency of ∼4 MHz (*33*). The remaining nqi features observed in Figure 7, the weak 2.4−2.6 MHz features, can be assigned as combination bands (*57, 61, 63*). The presence of such a feature indicates multiple magnetically equivalent ^{14}N nuclei at the Cu^{2+} center, consistent with the Cu^{2+} binding to several histidine ligands. Thus, in each bacterial species, modulations were observed that are characteristic of remote imidazole nitrogen−Cu interactions. The spectra indicate more than one histidine amino acid side chain is ligated to the Cu^{2+} in each RC species.

DISCUSSION

Light-induced electron-transfer chemistry in RC proteins is influenced by metal ions. The determination of the location and structure of the metal site(s) and surrounding anisotropic protein environment is inherent for elucidating the mechanism of metal-ion induced modulation of electron transfer. Herein, we provide the first experimental evidence for a Cu^{2+} surface metal site on isolated Fe-containing RCs from *Rb. capsulatus* and *Rps. viridis*, similar to the Cu^{2+} site observed for *Rb. sphaeroides* RCs (*11*). We have concomitantly interrogated the Cu^{2+} site electronic structure and response of the electron-transfer kinetics to Cu^{2+}, using a combination of magnetic resonance techniques and transient optical measurements.

The influence of metal ions on the $Q_A^-Q_B \rightarrow Q_AQ_B^-$ electron-transfer rates in the less well-characterized RCs of *Rps. viridis* and *Rb. capsulatus* provides evidence of the general nature of metal-ion induced regulation of electron transfer. In each species of RC the electrochromic response of the bacteriopheophytin cofactors associated with $Q_A^-Q_B \rightarrow Q_AQ_B^-$ electron-transfer and/or charge-compensating (proton-uptake) events is modulated by Cu^{2+}. In *Rb. sphaeroides* RCs, the heterogeneous kinetics of $Q_A^-Q_B \rightarrow Q_AQ_B^-$ have been well-characterized (*3, 5, 41*). The fast component was assigned to "pure" electron-transfer reaction (*3, 5*). Longer components have been assigned to electron-transfer processes kinetically limited by protonation and/or conformational events within the protein (*41*). The kinetics of *Rb. capsulatus* can be interpreted in a similar manner (*41*). In the case of *Rb. sphaeroides* and *Rb. capsulatus* RCs, the observed changes upon metal-binding reflect ∼2−3-fold reduction in the slowest component of $Q_A^-Q_B \rightarrow Q_AQ_B^-$

electron-transfer reaction. The observed Cu^{2+}-induced changes in the electrochromic response of *Rps. viridis* are more difficult to interpret. *Rps. viridis* data indicate a loss of the major fast kinetic component, representing a dramatic change in either or both electron-transfer and charge-compensation events involved in the $Q_A^-Q_B \rightarrow Q_AQ_B^-$ electron-transfer process. Thus, metal ion, specifically Cu^{2+}, appears to function universally in bacterial RCs to reduce the $Q_A^-Q_B \rightarrow Q_AQ_B^-$ electron-transfer rates and/or charge-compensation events relative to the native rates without metal present.

These results provide a basis for further interrogating the response of photosynthetic electron- and proton-transfer events to metal ions in different species of RCs. Metal ion binding studies may provide insight into conformational changes important for electron transfer as well as determination of a site of protein motion coupled to electron transfer. Like Zn^{2+}, perturbations induced by Cu^{2+} binding may slow conformational changes that are important for efficient $Q_A^-Q_B \rightarrow Q_AQ_B^-$ electron transfer (*9*). Upon stoichiometric Zn^{2+} binding, the rate of electron transfer is slowed, similar to the global effect of cooling to 2 °C RCs in the absence of Zn^{2+}, implying a change in protein dynamics due to a conformational change (*9*). In the absence of metal ion, the $Q_A^-Q_B \rightarrow Q_AQ_B^-$ electron-transfer step in RCs from *Rb. sphaeroides* involves a slow rate-limiting gating step (*16*) that involves the movement of Q_B before electron transfer (*8*). Other evidence suggests that the $Q_A^-Q_B \rightarrow Q_AQ_B^-$ electron transfer is limited by a conformational change (*5, 31, 32*). Stoichiometric metal ion binding may alter protein structure and dynamics (*9*), thereby indirectly modifying coupled conformational and/or protonation processes that kinetically limit $Q_A^-Q_B \rightarrow Q_AQ_B^-$ reactions (*10*). In general, metal ions in proteins can act to enforce a specific coordination environment, thereby restricting the mobility of the ligating amino acid side chains. Thus, these perturbations could potentially extend through the surrounding protein, restricting a region of polypeptide (*11*). Comparison of the RC structure with or without Cd^{2+} bound indicated structural changes in the metal ligands and a mobility difference in a specific residue, although no major structural protein rearrangements were observed. This residue, Glu-H173, has been proposed to be involved in the reduced rate of electron transfer (*15*). Subtler mobility changes or slight differences in the hydrogen-bond network would not be observed in a static crystal structure.

We have interrogated the dynamic solution Cu^{2+}-site structures with EPR spectroscopy. Comparison of the cw and ESEEM spectra obtained show that the Cu^{2+} surface site has a similar geometry and ligands in each species. Modulations were observed that are characteristic of remote imidazole nitrogen−Cu interactions, thus implicating histidine amino acid side chains as ligands to the Cu^{2+} when bound to the surface site in the three species of RC studied. Thus, RCs from *Rb. sphaeroides*, *Rb. capsulatus*, and *Rps. viridis* all have a structurally analogous surface Cu^{2+}-binding site, containing at least two histidine ligands, apparently involved in modulating the $Q_A^-Q_B \rightarrow Q_AQ_B^-$ electron-transfer process.

The amino acid sequences of each RC differ in the histidine-rich protein region proposed for the surface site. The crystal structure for *Rb. sphaeroides* RCs shows that Zn^{2+} and Cd^{2+} are ligated to two histidines, H126 and H128, and an aspartate acid residue, H124 (*15*). These residues are conserved in *Rb. capsulatus* (H127, H129, H131) (*24*) but not conserved in *Rps. viridis* (*69*). Inspection of the *Rps. viridis* crystal structure reveals four potential histidine ligands from three different subunits (M16, H178, H72, and L211) located beneath the Q_B binding pocket (*18, 19*). The location of these histidines is surprisingly similar to the grouping of four histidine residues (H68, H126, H128, and L211) observed in the *Rb. sphaeroides* RC crystal structure (*12*−*14*). Due to the similar response of $Q_A^-Q_B \rightarrow Q_AQ_B^-$ electron-transfer process to both Cu^{2+} and Zn^{2+}, we believe that these metals bind to an analogous region of the RC. However, the possibility also exists that Cu^{2+} binds to a distinct site from Zn^{2+}. It is striking that the structures of both *Rps. viridis* and *Rb. sphaeroides* RC reveal *four* histidine ligands in the protein region beneath Q_B. Two histidines, H72 and H211 from *Rps. viridis* and H68 and L211 from *Rb. sphaeroides*, are conserved, and these residues should not be overlooked as potential ligands for the Cu^{2+} and potentially other metal ions.

In addition to conformational changes associated with electron-transfer events, locating the metal site may provide information about the proton pathways in RCs from *Rb. capsulatus* and *Rps. viridis*. Similar studies have been instrumental in elucidating the proton pathway into the Q_B site in *Rb. sphaeroides* RCs (*10, 15, 17*). Q_B is buried in the protein interior. Thus, to reach Q_B the proton must be transported from the aqueous exterior solution through a low-dielectric protein environment via a network of proton donor and acceptor groups linked by hydrogen bonds with favorable pK_a values (*26*). Although the crystal structure has been determined for *Rps. viridis*, more biophysical characterization of proton uptake has been carried out with the structurally uncharacterized *Rb. capsulatus*. Site-directed mutagenesis in RCs of *Rb. capsulatus* and *Rb. sphaeroides* suggests similar functional involvement of specific residues, Ser L233, Asp L213, and Glu L212, in the electron-transfer-coupled proton-uptake reactions (for reviews, see refs *70* and *71*). Interestingly, a potential metal ligand, His L211, is located in this region and is conserved in all three species. The functional proton pathways must be different in RCs of *Rb. sphaeroides* and *Rps. viridis*, as several key residues are not conserved between the two species (*27*). Specifically, *Rps. viridis* RCs lack Asp L213, but an Asp at M43 is thought to act in its place (*26*). Interestingly, in the *Rps. viridis* structure Asp M43 is close to two histidine residues, H178 and H16, which could possibly be the histidines coupled to Cu^{2+} observed with ESEEM spectroscopy.

In summary, a structurally analogous Cu^{2+} site that apparently functions to modulate electron transfer is universally found in bacterial RCs from *Rb. sphaeroides*, *Rb. capsulatus*, and *Rps. viridis*. Furthermore, although the proton pathways must be different in RCs from different bacterial strains, each RC shares a common histidine region that may be involved in proton uptake. Other photosynthetic systems are inhibited by metal ions, primarily Cu^{2+}, at the level of electron transfer. Cu^{2+} has been shown to inhibit electron transport in higher plants; the primary interaction is thought to be with photosystem II (*72*−*76*) but it also interacts with PSI (*77*), the cyt b_6f complex (*78*), and ferredoxin (*79*). A recent paper has shown that Cu^{2+} inhibits electron transfer through the isolated spinach cyt b_6f complex possibly by a Cu^{2+}-induced protein conformational change (*80*). Thus,

spectroscopic characterization of the Cu^{2+} sites in RCs from different species may provide a means to elucidate a generalized mechanism of metal-ion induced regulation of photosynthetic electron transfer and proton uptake as well as determine a localized anisotropic protein environment involved in controlling protein dynamics important for electron transfer.

ACKNOWLEDGMENT

We thank P. Laible and S. Garcia for technical assistance.

REFERENCES

1. Shinkarev, V. P., and Wraight, C. A. (1993) in *The Photosynthetic Reaction Center* (Deisenhofer, J., and Norris, J. R., Eds.) pp 193−255, Academic Press, Inc., San Diego, CA.
2. Parson, W. W. (1987) in *Photosynthesis* (Amesz, J., Ed.) pp 43−61, Elsevier, New York.
3. Li, J., Gilroy, D., Tiede, D. M., and Gunner, M. R. (1998) *Biochemistry 37*, 2818−2829.
4. Mancino, L., Dean, D., and Blankenship, R. (1984) *Biochim. Biophys. Acta 764*, 46−54.
5. Tiede, D. M., Vazquez, J., Cordova, J., and Marone, P. A. (1996) *Biochemistry 35*, 10763−10775.
6. Brzezincki, P., Okamura, M. Y., and Feher, G. (1992) in *The Photosynthetic Reaction Center II* (Breton, J., and Vermeglio, A., Eds.) pp 321−330, Plenum Press, New York.
7. Graige, M., Feher, G., and Okamura, M. (1996) *Biophys. J. 70*, SUAM4.
8. Graige, M. S., Feher, G., and Okamura, M. Y. (1998) *Proc. Natl. Acad. Sci. U.S.A. 95*, 11679−11684.
9. Utschig, L. M., Ohigashi, Y., Thurnauer, M. C., and Tiede, D. M. (1998) *Biochemistry 37*, 8278−8281.
10. Paddock, M. L., Graige, M. S., Feher, G., and Okamura, M. Y. (1999) *Proc. Natl. Acad. Sci. U.S.A. 96*, 6183−6188.
11. Utschig, L. M., Poluektov, O., Tiede, D. M., and Thurnauer, M. C. (2000) *Biochemistry 39*, 2961−2969.
12. Ermler, U., Fritzsch, G., Buchanan, S., and Michel, H. (1994) *Structure 2*, 925−936.
13. El-Kabbani, O., Chang, C.-H., Tiede, D. M., Norris, J., and Schiffer, M. (1991) *Biochemistry 30*, 5361−5369.
14. Allen, J. P., Feher, G., Yeates, T. O., Komiya, H., and Rees, D. C. (1988) *Proc. Natl. Acad. Sci. U.S.A. 85*, 8487−8491.
15. Axelrod, H. L., Abresch, E. C., Paddock, M. L., Okamura, M. Y., and Feher, G. (2000) *Proc. Natl. Acad. Sci. U.S.A. 97*, 1542−1547.
16. Stowell, M. H. B., McPhillips, T. M., Rees, D. C., Soltis, S. M., Abresch, E., and Feher, G. (1997) *Science 276*, 812−816.
17. Paddock, M. L., Feher, G., and Okamura, M. Y. (2000) *Proc. Natl. Acad. Sci. U.S.A. 97*, 1548−1553.
18. Deisenhofer, J., Epp, O., Miki, K., Huber, R., and Michel, H. (1985) *Nature 318*, 618−624.
19. Deisenhofer, J., Epp, O., Miki, K., Huber, R., and Michel, H. (1984) *J. Mol. Biol. 180*, 385−398.
20. Deisenhofer, J., and Michel, H. (1989) *EMBO J. 8*, 2149−2169.
21. Deisenhofer, J., Epp, O., Sinning, I., and Michel, H. (1995) *J. Mol. Biol. 246*, 429−457.
22. Sebban, P., Maroti, P., and Hanson, D. K. (1995) *Biochimie 77*, 677−694.
23. Coleman, W. J., and Youvan, D. C. (1990) *Annu. Rev. Biophys. Biophys. Chem. 19*, 333−367.
24. Youvan, D. C., Bylina, E. J., Alberti, M., Begusch, H., and Hearst, J. E. (1984) *Cell 37*, 949−957.
25. Foloppe, N., Ferrand, M., Breton, J., and Smith, J. C. (1995) *Proteins: Struct., Funct., Genet. 22*, 226−244.
26. Okamura, M. Y., Paddock, M. L., Graige, M. S., and Feher, G. (2000) *Biochim. Biophys. Acta 1458*, 148−163.
27. Michel, H., Weyer, K. A., Gruenberg, H., Dunger, I., Oesterhelt, D., and Lottspeich, F. (1986) *EMBO J. 5*, 1149−1158.
28. Lancaster, C. R. D., and Michel, H. (1997) *Structure 5*, 1339−1359.
29. Hanson, D. K., Nance, S. L., and Schiffer, M. (1992) *Photosynth. Res. 32*, 147−153.
30. Nabedryk, E. (1999) *Biochim. Biophys. Acta 1411*, 206−213.
31. Alexov, E. G., and Gunner, M. R. (1999) *Biochemistry 38*, 8253−8270.
32. Rabenstein, B., Ullmann, G. M., and Knapp, E.-W. (2000) *Biochemistry 39*, 10487−10496.
33. Mims, W. B., and Peisach, J. (1979) in *Biological Applications of Magnetic Resonance* (Shulman, R. G., Ed.) pp 221−270, Academic Press, New York.
34. Mims, W. B., and Peisach, J. (1981) in *Biological Magnetic Resonance* (Berliner, L. J., and Reuben, J., Eds.) pp 213−263, Plenum, New York.
35. Peisach, J. (1993) in *Bioinorganic Chemistry of Copper* (Karlin, K. D., and Tyeklar, Z., Eds.) pp 21−33, Chapman & Hall, New York.
36. Mims, W. B., and Peisach, J. (1978) *J. Chem. Phys. 69*, 4921−4930.
37. Den Blanken, H. J., and Hoff, A. J. (1982) *Biochim. Biophys. Acta 681*, 365−374.
38. Laible, P. D., Zhang, Y., Morris, A. L., Snyder, S. W., Ainsworth, C., Greenfield, S. R., Wasielewski, M. R., Parot, P., Schoepp, B., Schiffer, M., Hanson, D. K., and Thurnauer, M. C. (1997) *Photosynth. Res. 52*, 93−103.
39. Utschig, L. M., Greenfield, S. R., Tang, J., Laible, P. D., and Thurnauer, M. C. (1997) *Biochemistry 36*, 8548−8558.
40. Gardiner, A. T., Zech, S. G., MacMillan, F., Kass, H., Bittl, R., Schlodder, E., Lendzian, F., and Lubitz, W. (1999) *Biochemistry 38*, 11773−11787.
41. Tiede, D. M., Utschig, L., Hanson, D. K., and Gallo, D. M. (1998) *Photosynth. Res. 55*, 267−273.
42. Baciou, L., Bylina, E. J., and Sebban, P. (1993) *Biophys. J. 65*, 652−660.
43. Shopes, R. J., and Wraight, C. A. (1985) *Biochim. Biophys. Acta 806*, 348−356.
44. Leibl, W., Sinning, I., Ewald, G., Michel, H., and Breton, J. (1993) *Biochemistry 32*, 1958−1964.
45. Mathis, P., Sinning, I., and Michel, H. (1992) *Biochim. Biophys. Acta 1098*, 151−158.
46. Peisach, J., and Blumberg, W. E. (1974) *Arch. Biochem. Biophys. 165*, 691−708.
47. Vänngård, T. (1972) in *Biological Applications of Spin Resonance* (Swartz, H. M., Bolton, J. R., and Borg, D. C., Eds.) pp 411−447, Wiley-Interscience, New York.
48. Hathaway, B. J., and Billing, D. E. (1970) *Coord. Chem. Rev. 5*, 143.
49. Solomon, E. I., Penfield, K. W., and Wilcox, D. E. (1983) in *Structure and Bonding*, pp 3−57, Springer-Verlag, Berlin.
50. Buchanan, S. K., and Dismukes, G. C. (1987) *Biochemistry 26*, 5049−5055.
51. Feher, G., Isaacson, R. A., Debus, R. J., and Okamura, M. Y. (1986) *Biophys. J. 49*, 585a.
52. Calvo, R., Passeggi, M. C. G., Isaacson, R. A., Okamura, M. Y., and Feher, G. (1990) *Biophys. J. 58*, 149−165.
53. Colaneri, M., and Peisach, J. (1992) *J. Am. Chem. Soc. 114*, 5335−5341.
54. Colaneri, M. J., and Peisach, J. (1995) *J. Am. Chem. Soc. 117*, 6308−6315.
55. Place, C., Zimmermann, J.-L., Mulliez, E., Guillot, G., Bois, C., and Chottard, J.-C. (1998) *Inorg. Chem. 37*, 4030−4039.
56. Mims, W. B., and Peisach, J. (1976) *Biochemistry 15*, 3863−3869.
57. Kosman, D., Peisach, J., and Mims, W. B. (1980) *Biochemistry 19*, 1304−1308.
58. Avigliano, L., Davis, J. L., Graziani, M. T., Marchesini, A., Mims, W. B., Mondovi, B., and Peisach, J. (1981) *FEBS Lett. 136*, 80−84.
59. Mondovi, B., Morpurgo, L., Agostinelli, E., Befani, O., McCracken, J., and Peisach, J. (1987) *Eur. J. Biochem. 168*, 503−507.
60. McCracken, J., Desai, P. R., Papdopoulos, N. J., Villafranca, J. J., and Peisach, J. (1988) *Biochemistry 27*, 4133−4137.

61. McCracken, J., Pember, S., Benkovic, S. J., Villafranca, J. J., Miller, R. J., and Peisach, J. (1988) *J. Am. Chem. Soc. 110*, 1069−1074.
62. Jiang, F., McCracken, J., and Peisach, J. (1990) *J. Am. Chem. Soc. 112*, 9035−9044.
63. Lu, J., Bender, C. J., McCracken, J., Peisach, J., Sevens, J. C., and McMillin, D. R. (1992) *Biochemistry 31*, 6265−6275.
64. Gurbiel, R. J., Peoples, R., Doan, P. E., Cline, J. F., McCracken, J., Peisach, J., Hoffman, B. M., and Valentine, J. S. (1993) *Inorg. Chem. 32*, 1813−1819.
65. Bubacco, L., Magliozzo, R. S., Wirt, M. D., Beltramini, M., Salvato, B., and Peisach, J. (1995) *Biochemistry 34*, 1524−1533.
66. Elliott, S. J., Randall, D. W., Britt, R. D., and Chan, S. I. (1998) *J. Am. Chem. Soc. 120*, 3247−3248.
67. van Gastel, M., Coremans, J. W. A., Jeuken, L. J. C., Canters, G. W., and Groenen, E. J. J. (1998) *J. Phys. Chem. A 102*, 4462−4470.
68. Flanagan, H. L., and Singel, D. J. (1987) *J. Chem. Phys. 87*, 5606−5616.
69. Michel, H., Weyer, K. A., Gruenberg, H., and Lottspeich, F. (1985) *EMBO J. 4*, 1667−1672.
70. Okamura, M. Y., and Feher, G. (1995) in *Anoxygenic Photosynthetic Bacteria* (Blankenship, R. E., Madigan, M. T., and Bauer, C. E., Eds.) pp 577−594, Kluwer, Dordrecht, The Netherlands.
71. Takahashi, E., and Wraight, C. A. (1994) in *Advances in Molecular and Cell Biology* (Barber, J., Ed.) pp 197−251, JAI Press, Greenwich, CT.
72. Yruela, I., Alfonso, M., Ortiz de Zarate, I., Montoya, G., and Picorel, R. (1993) *J. Biol. Chem. 268*, 1684−1689.
73. Schröder, W. P., Arellano, J. B., Bittner, T., Baron, M., Eckert, H., and Renger, G. (1994) *J. Biol. Chem. 269*, 32865−32870.
74. Barón, M., Arellano, J. B., and López-Gorgé, J. (1995) *Physiol. Plant 94*, 174−180.
75. Jegerschöld, C., Arellano, J. B., Schröder, W. P., van Kan, P. J. M., Barón, M., and Styring, S. (1995) *Biochemistry 35*, 12747−12758.
76. Yruela, I., Gatzen, G., Picorel, R., and Holzwarth, A. R. (1996) *Biochemistry 35*, 9469−9474.
77. Bohner, H., Bohme, H., and Boger, P. (1980) *Biochim. Biophys. Acta 592*, 103−112.
78. Singh, D., and Singh, S. P. (1987) *Plant Physiol. 83*, 12−14.
79. Shioi, Y., Tamai, H., and Sasa, T. (1978) *Plant Cell Physiol. 19*, 203−229.
80. Rao, B. K., S., Tyryshkin, A. M., Roberts, A. G., Bowman, M. K., and Kramer, D. M. (2000) *Biochemistry 39*, 3285−3296.

BI0029191